Production of $\gamma\gamma$ pairs in a hot quark-gluon plasma and shielding of the quark mass singularity

R. Baier
Fakultät für Physik, Universität Bielefeld, 4800 Bielefeld 1, Germany

H. Nakkagawa
Fakultät für Physik, Universität Bielefeld, 4800 Bielefeld 1, Germany and Institute for Natural Science, Nara University, Nara 631, Japan

A. Niégawa
Fakultät für Physik, Universität Bielefeld, 4800 Bielefeld 1, Germany and Department of Physics, Osaka City University, Osaka 558, Japan

K. Redlich
Fakultät für Physik, Universität Bielefeld, 4800 Bielefeld 1, Germany and Department of Theoretical Physics, University of Wroclaw, Wroclaw, Poland
(Received 2 December 1991)

We study the thermal production of large-invariant-mass photon pairs emitted from a quark-gluon plasma at high temperature. To lowest order in perturbation theory the cross section for the annihilation process ($q\bar{q}\to\gamma\gamma$) is known to lead to logarithmically divergent thermal production rates for massless quarks. We apply recently developed resummation methods of finite-temperature perturbation theory and show how screening effects on quarks in the plasma provide finite thermal rates for $\gamma\gamma$ pairs. We compare these results with previous estimates of $\gamma\gamma$ production rates. Finally, for the phenomenology of heavy-ion collisions we present the screened $\gamma\gamma$ emission spectra by taking into account the space-time history of these collisions.

PACS number(s): 12.38.Mh, 12.38.Cy, 25.75.+r

I. INTRODUCTION

In the framework of finite-temperature perturbation theory [1] the recently developed resummation method of hard thermal loops [2] allows one to compute screening effects in hot gauge theories. This is of crucial importance when discussing signatures for a quark-gluon plasma expected to be produced in ultrarelativistic heavy-ion collisions [3]. Recently, it has been shown that the thermal emission rate for energetic direct photons indeed becomes infrared safe in a leading-order calculation: the quark mass singularities are shielded by thermal (Landau damping) effects [4–6].

In this paper we extend this analysis to another process involving hard photons, namely to the thermal production of photon pairs with large invariant masses and at high temperature T. The relevance of observing $\gamma\gamma$ pairs—in addition to single hard photons [7]—for detecting a possible quark-gluon plasma has already been pointed out a couple of times [8–12].

Thermal photon pairs are emitted mainly via quark-antiquark annihilation ($q\bar{q}\to\gamma\gamma$) with quark exchange. For massless quarks the tree-level prediction for the thermal rate is (logarithmically) divergent, as is the case for single-photon production.

In the following we discuss an explicit calculation that demonstrates that again this mass singularity is shielded in a quark-gluon plasma at high temperatures, as a consequence of Landau damping after resummation of hard thermal-loop corrections to the quark propagator. As a result, however, the thermal $\gamma\gamma$ rate becomes logarithmically dependent on the strong coupling constant.

This paper is organized as follows. In Sec. II we start from the tree-level process for thermal photon-pair production and calculate the contribution due to the exchange of quarks with hard momentum transfer. In Sec. III the corresponding soft contribution is derived by applying resummed thermal perturbation theory at leading order and large temperature. We do the calculation using the real-time approach. In Sec. IV we add the hard and the soft contributions to obtain our main result for the rate of photon pairs with large invariant masses. We show that it is well behaved in the limit of vanishing quark masses. A comparison with previously derived results is included. Transverse momentum and angular distributions of the photon pairs are presented in Sec. V. Section VI is devoted to the thermal spectra for $\gamma\gamma$ pairs when they are produced in ultrarelativistic heavy-ion collisions. We assume a first-order phase transition from hadronic matter to a quark-gluon plasma and a longitudinal expansion of the excited matter system. The results are briefly summarized in Sec. VII.

II. THERMAL RATE—HARD CONTRIBUTION

The hard part of the thermal rate for photon pairs produced in the quark-gluon plasma is calculated from first-order perturbation theory. The lowest-order Born pro-

cess is quark-antiquark annihilation

$$q(p)+\bar{q}(p')\rightarrow\gamma(k)+\gamma(k') \ . \tag{2.1}$$

The Feynman diagrams for the corresponding amplitudes are shown in Fig. 1.

We first calculate the emission rate that results from this process by assuming that the Born approximation is valid over the whole phase space. This is the usual approximation that has been treated so far in the literature [8–12].

The invariant rate due to this annihilation process for one quark flavor with charge e_q and N_c color degrees of freedom is given by

$$W^{\gamma\gamma}|_{\text{Born}}=\frac{1}{2}\frac{e_q^4\alpha^2}{2\pi^6}N_c\int\frac{d^3k}{2\omega}\int\frac{d^3k'}{2\omega'}\int\frac{d^3p}{2E}\,n_F(E)\int\frac{d^3p'}{2E'}\,n_F(E')\delta^4(p+p'-k-k')\left[\frac{u}{t-m^2}+\frac{t}{u-m^2}\right] , \tag{2.2}$$

with the Mandelstam variables

$$s=(k+k')^2 \ , \quad t=(p-k)^2 \ , \quad s+t+u=0 \ ,$$

and with $\omega=k^0$, $\omega'=k'^0$, $E=p^0$, and $E'=p'^0$. The factor $\frac{1}{2}$ takes care of the identical photons in the final state. Only in the propagators, we introduce the dependence on the mass parameter m as an infrared cutoff in order to keep the expressions finite in the intermediate steps of the calculation; otherwise, the quarks are treated as massless. Finally the limit $m\rightarrow 0$ is taken. The integral of Eq. (2.2) is worked out by first transforming to s and t integrations as described in the literature [13]. In the following we concentrate on the limit of large invariant photon-pair masses $\sqrt{s}=M>T$, and we only explore the emission rate in leading order in T/M. Therefore we replace the Fermi distribution $n_F(E)=(e^{E/T}+1)^{-1}$ by the Maxwell-Boltzmann one, $n_{MB}(E)=e^{-E/T}$, since we checked that this replacement amounts to neglecting nonleading terms.

We note from Fig. 1 and from Eq. (2.2) that there are two contributions, i.e., with the quark exchanged in the t and u channels, respectively. For massless quarks the interference term vanishes. Furthermore, the two terms contribute the same amount to the rate: it is therefore sufficient to calculate twice the t-channel contribution,

$$W^{\gamma\gamma}|_{\text{Born}}\simeq\frac{e_q^4\alpha^2}{16\pi^4}N_c\int_0^\infty ds\int_{-s}^0 dt\int\frac{d^3k}{\omega^2}\int_{z_{\min}}^\infty dz\,e^{-z/T}\frac{u}{s(t-m^2)} \ , \tag{2.3}$$

with

$$z_{\min}=\frac{s}{4\omega}+\omega \ , \quad \omega=|\mathbf{k}| \ .$$

Performing the integrations with respect to t and z, we obtain the rate with respect to the invariant mass M

$$\left.\frac{dW^{\gamma\gamma}}{dM^2}\right|_{\text{Born}}\simeq\frac{e_q^4\alpha^2}{4\pi^3}N_cT\left[\ln\frac{M^2}{m^2}-1\right]\times\int_o^\infty d\omega\exp\left[-\left[\omega+\frac{M^2}{4\omega}\right]\Big/T\right] \tag{2.4}$$

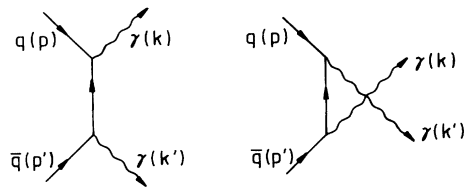

FIG. 1. Lowest-order Feynman diagrams for quark (q) - antiquark ($\bar{q}$) annihilation producing real photons with momenta k and k'.

for $M\gg m$. In the limit $M\gg T$ the saddle-point method—with the saddle point at $\omega=M/2$—gives

$$\left.\frac{dW^{\gamma\gamma}}{dM^2}\right|_{\text{Born}}\simeq\frac{e_q^4\alpha^2}{4\pi^3}N_c\left[\frac{\pi MT^3}{2}\right]^{1/2}\times\left[\ln\frac{M^2}{m^2}-1\right]\exp(-M/T) \ , \tag{2.5}$$

when terms of $O(T/M)$ are neglected. A singular logarithmic mass behavior is present in (2.5), clearly showing that massless-quark exchange leads to an infinite rate at the tree-level order of the perturbative expansion. Therefore in the estimates given in the literature [8–12] a definite nonvanishing (but in general small) value for the regulator mass m of the light quarks has to be included.

In the next step we follow Braaten and co-workers [14] and introduce an arbitrary momentum scale q^*, which allows to distinguish a hard ($\tilde{q}>q^*$) from a soft ($\tilde{q}<q^*$) region with respect to the momentum transfer $|\mathbf{q}|\equiv\tilde{q}$ of the

exchanged quark. This scale is chosen as $g_s T \ll q^* \ll T$ and $q^* \gg m$. Obviously the strong coupling constant g_s—assumed to be small to allow for the latter approximations—fixes the soft scale, because of the strong interactions of quarks propagating in the plasma. In the following we estimate the soft part in lowest-order perturbation theory (Fig. 1). As stated before we do it via the t-channel diagram and double the result,

$$\left.\frac{dW^{\gamma\gamma}}{dM^2}\right|_{\text{Born,soft}} = \frac{e_q^4\alpha^2}{2\pi^6} N_c \int d^4q\, \theta(q^*-\tilde{q}) \left[\frac{M^2+q^2}{m^2-q^2}\right] \int \frac{d^3k}{2\omega} \int \frac{d^3k'}{2\omega'} \int \frac{d^3p}{2E} n_F(E) \times \int \frac{d^3p'}{2E'} n_F(E')\delta^4(p+p'-k-k')\delta^4(p-k+q)\delta(M^2-(k+k')^2) , \tag{2.6}$$

with $q^2=t$. Again m is kept as infrared cutoff.

For large values of M the only important kinematical region is where the momenta k and k' (p and p') are both hard, but the transfer q is soft, e.g., $p_\mu \simeq k_\mu$, $p^2 \simeq -2k\cdot q$. In the other cases, when one momentum is soft then the Fermi factor n_F in (2.6) suppresses exponentially this configuration.

Performing the integrations with respect to the quark momenta p and p', we find in this soft approximation,

$$\left.\frac{dW^{\gamma\gamma}}{dM^2}\right|_{\text{Born,soft}} \simeq \frac{e_q^4\alpha^2}{8\pi^6} N_c \int d^4q\, \theta(q^*-\tilde{q}) \left[\frac{M^2}{m^2-q^2}\right] \int \frac{d^3k}{2\omega} \int \frac{d^3k'}{2\omega'} e^{-(\omega+\omega')/T} \delta(k\cdot q)\delta(k'\cdot q)\delta(M^2-2k\cdot k') . \tag{2.7}$$

The constraints $\delta(k\cdot q)$ and $\delta(k'\cdot q)$ require a momentum transfer to be spacelike, $|q_0|/\tilde{q} \le 1$. We perform the angular integrations and obtain

$$\left.\frac{dW^{\gamma\gamma}}{dM^2}\right|_{\text{Born,soft}} \simeq \frac{e_q^4\alpha^2}{8\pi^4} N_c \int_0^{q^*} d\tilde{q} \int_{-\tilde{q}}^{\tilde{q}} dq_0 \frac{I(\tilde{M})}{(m^2-q_0^2+\tilde{q}^2)} , \tag{2.8}$$

where

$$I(\tilde{M}) = \tilde{M}^2 \int_{tt'\ge 1} \frac{dt\,dt'}{\sqrt{tt'-1}} e^{-(\tilde{M}/2T)(t+t')} = 2\pi T \tilde{M} \exp(-\tilde{M}/T) , \tag{2.9}$$

with

$$\tilde{M}^2 = M^2/[1-(q^0/\tilde{q})^2] . \tag{2.10}$$

Introducing the scaled variable $x = q_0/\tilde{q}$ the $\tilde{q}$ integration is performed and Eq. (2.8) becomes

$$\left.\frac{dW^{\gamma\gamma}}{dM^2}\right|_{\text{Born,soft}} \simeq \frac{e_q^4\alpha^2}{4\pi^3} N_c TM \int_0^1 dx \exp\left[-\frac{M}{T(1-x^2)^{1/2}}\right] \frac{\ln[1+q^{*2}(1-x^2)/m^2]}{(1-x^2)^{3/2}} . \tag{2.11}$$

For $M/T \gg 1$ the stationary point at $x=0$ gives the leading term

$$\left.\frac{dW^{\gamma\gamma}}{dM^2}\right|_{\text{Born,soft}} \simeq \frac{e_q^4\alpha^2}{4\pi^3} N_c TM \ln\frac{q^{*2}}{m^2} \exp(-M/T) \int_0^\infty dx\, e^{-(M/2T)x^2} \simeq \frac{e_q^4\alpha^2}{4\pi^3} N_c \left[\frac{\pi MT^3}{2}\right]^{1/2} \ln\frac{q^{*2}}{m^2} \exp(-M/T) . \tag{2.12}$$

Now we subtract this soft contribution (2.12) from Eq. (2.5) to obtain the hard contribution in the kinematical regime $\tilde{q} > q^*$ due to the hard quark exchange in the annihilation process of Fig. 1. The hard $\gamma\gamma$ emission rate for large invariant masses ($M > T$) is

$$\left.\frac{dW^{\gamma\gamma}}{dM^2}\right|_{\text{hard}} \equiv \left.\frac{dW_{\gamma\gamma}}{dM^2}\right|_{\text{Born}} - \left.\frac{dW^{\gamma\gamma}}{dM^2}\right|_{\text{Born,soft}} \simeq \frac{e_q^4\alpha^2}{4\pi^3} N_c \left[\frac{\pi MT^3}{2}\right]^{1/2} \left[\ln\frac{M^2}{q^{*2}} - 1\right] \exp(-M/T) . \tag{2.13}$$

Indeed the terms proportional to $\ln m$ cancel, such that the soft behavior is controlled by the arbitrary momentum cutoff q^*: this cancellation is the first indication that the separation of hard versus soft regions in terms of a three-momentum cutoff q^* indeed works properly. The potentially dangerous light-cone region, $q_0^2 - \tilde{q}^2 < q^{*2}$ and $\tilde{q} > q^*$, does not give rise to a logarithmic dependence on q^*.

III. THERMAL RATE—SOFT CONTRIBUTION

In order to calculate the soft contribution to the thermal rate for photon pairs from a hot quark-gluon plasma we apply the results of the resummed perturbative expansion for hard thermal loops in the high-T limit [2]. Since we concentrate on photon pairs with large invariant masses the dominant corrections are expected for

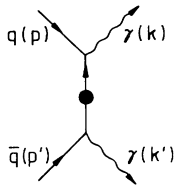

FIG. 2. Quark (q)-antiquark ($\bar{q}$) annihilation diagram with an effective thermal quark propagator in the t channel.

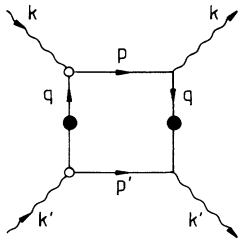

FIG. 3. Effective one-loop diagram for the production of a pair of real photons with momenta k and k'. The open circles show the way the diagram is cut. The effective thermal quark propagator is indicated by a blob.

soft propagators, i.e., on the quark propagator exchanged in the annihilation process: in the soft kinematical region $\tilde{q} < q^*$ the diagram expected to become dominant—as the t-channel contribution—is shown in Fig. 2, in which an effective dressed quark propagator replaces the bare one in the corresponding graph in Fig. 1. It is also expected that no effective vertices have to be included in the present case. All these expectations are discussed more explicitly below.

For the actual calculation of the emission rate of photon pairs from a quark-gluon plasma we follow the procedure, originally proposed by Weldon [15]. We use the algorithm [16] for evaluating general finite-temperature reaction rates, which is formulated in terms of circled diagrams [17]. The $\gamma\gamma$ rate is represented as

$$W^{\gamma\gamma}=\frac{1}{2(2\pi)^6}\int\frac{d^3k}{2\omega}\int\frac{d^3k'}{2\omega'}A(k,k')\ , \tag{3.1}$$

where A is evaluated through the following rules [16]: (i) draw all possible Feynman diagrams for the forward process $\gamma(k)\gamma(k')\to\gamma(k)\gamma(k')$, (ii) two external vertices to which the initial (final) photon lines are attached are of the circled (uncircled) type, (iii) concerning internal vertices perform the sum over all possible circlings (including no circling at all), (iv) assign thermal propagators and vertices as specified in Ref. [17].

At tree level the amplitude A is represented by two box-type circled diagrams. One is shown in Fig. 3; however, only bare quark lines should be inserted; the crossed diagram is obtained from Fig. 3 by interchanging the final-state photons. According to the amplitude approach this crossed diagram corresponds to the interference term of the t- and u- channel diagrams in Fig. 1: as mentioned in Sec. II its contribution vanishes at the tree level.

In order to calculate the *genuine* soft contribution to the thermal $\gamma\gamma$ production rate we have to sum [2] all possible higher-order terms at leading order in the strong coupling constant, i.e., all the hard thermal-loop contributions: internal lines with soft momenta and vertices with all attached lines carrying soft momenta are identified by effective propagators and vertices, respectively, which include the hard thermal-loop corrections. The systematic resummation technique of hard thermal loops [2] is proven to work in the imaginary-time formalism (an independent discussion in the real-time framework is given by Lebedev and Smilga [18]). In the case of $\gamma\gamma$ production, however, we are not able to start our discussion [Eq. (3.1)] in the imaginary-time formulation, because to continue the four-point function A from Euclidean to Minkowski space is not straightforward. Therefore we use the real-time formalism from the beginning, and simply apply and extend the results derived by the resummation method in the imaginary-time approach. Although we cannot give a rigorous proof of the validity of this procedure, we nevertheless show that the $\gamma\gamma$ production rates obtained in this way are free from quark mass singularities. This result may justify our procedure.

As already pointed out the kinematical region of our interest is the one of large invariant masses M of the $\gamma\gamma$ pairs. Then, as explained in Sec. II, due to the Fermi distribution factor of the thermal quarks the dominant contribution to $A(k,k')$ is obtained when both outgoing photons as well as the internal quark lines p and p' in Fig. 3 (and its crossed counterpart) are hard. In this case the contribution of the crossed diagram turns out to be nonleading, and it is therefore neglected. Also, no hard thermal-loop corrections to the vertices have to be included, because at least two momenta joined at the vertex are hard. Therefore at the effective one-loop level the dominant amplitude in Eq. (3.1) is given by the Feynman diagram shown in Fig. 3. Adding the box diagram with the opposite charge flow, the result from Fig. 3 should be doubled, and we get

$$\left.\frac{dW^{\gamma\gamma}}{dM^2}\right|_{\text{soft}}=-\frac{e_q^4\alpha^2}{4\pi^4}N_c\int\frac{d^3k}{2\omega}\int\frac{d^3k'}{2\omega'}\delta(M^2-(k+k')^2)$$

$$\times\int\frac{d^4q}{(2\pi)^4}\theta(q^*-\tilde{q})\,\mathrm{tr}[\gamma_\mu i^*S_{22}(q)\gamma_\nu iS^-(p)\gamma^\nu i^*S_{11}(q)\gamma^\mu iS^+(-p')]\ , \tag{3.2}$$

with $p=k+q$ and $p'=k'-q$. The step function θ takes care of the separation between soft and hard momenta as discussed in the previous section. The photon polarizations are summed according to

$$\sum_{\text{pot}} \epsilon_\mu(k)\epsilon_\nu(k) = -g_{\mu\nu} \ . \tag{3.3}$$

Summing instead only the two transverse polarizations we find the same final result when terms of $O(T/M)$ are consistently dropped.

The bare thermal propagators for massless fermions are

$$iS^{\pm}(q) = 2\pi \not{q}[\theta(\pm q^0) - n_F(|q^0|)]\delta(q^2) \ , \tag{3.4}$$

where $S^+(q)$ $[S^-(q)]$ is inserted into the graph when the momentum q is flowing towards [away from] a circled vertex and away from [towards] an uncircled one [17].

For the lines connecting either circled or uncircled vertices (Fig. 3) the complete dressed fermion propagators have to be used. In terms of the complex self-energy function Σ they are expressed as [19]

$$i^*S_{11}(q) = [1-n_F(|q^0|)]\left[\frac{i}{\not{q}-\Sigma(q)+i\epsilon}\right] - n_F(|q^0|)\left[\frac{-i}{\not{q}-\Sigma^*(q)-i\epsilon}\right] \tag{3.5}$$

and

$$i^*S_{22}(q) = [i^*S_{11}(q)]^* \ , \tag{3.6}$$

where the complex conjugation does not affect the Dirac matrices. Putting $\Sigma=0$ the bare propagators appearing in circled diagrams and familiar from the 2×2 matrix structure in the real-time formalism are recovered [1].

Klimov [20] and Weldon [21] first calculated the thermal one-loop quark self-energy function. Its properties have also been extensively discussed by Pisarski [22]. The leading term in T, which is gauge invariant, dominating at soft momentum q and originating from the hard thermal loop [2] is

$$\frac{1}{\not{q}-\Sigma(q^0,q)+i\epsilon} = -\tfrac{1}{2}(\gamma^0-\boldsymbol{\gamma}\cdot\hat{\mathbf{q}})\frac{1}{D_+(q^0,q)} - \tfrac{1}{2}(\gamma^0+\boldsymbol{\gamma}\cdot\hat{\mathbf{q}})\frac{1}{D_-(q^0,q)} \ , \tag{3.7}$$

where

$$\hat{\mathbf{q}} = \mathbf{q}/\tilde{q} \ .$$

The fermionic excitations contain modes with a positive as well as a negative helicity to chirality ratio. They are determined by the two functions

$$D_\pm(q^0,q) = -q^0 \pm \tilde{q} + \frac{m_f^2}{2\tilde{q}}\left[\left(1 \mp \frac{q^0}{\tilde{q}}\right)\ln\frac{q^0+\tilde{q}}{q^0-\tilde{q}} \pm 2\right] . \tag{3.8}$$

The fermion mass induced by temperature is for QCD given by

$$m_f^2 = g_s^2 C_F T^2/8 = \frac{2\pi}{3}\alpha_s T^2 \ , \tag{3.9}$$

in terms of the strong coupling $\alpha_s = g_s^2/4\pi$. Below the light cone—the important region for the processes with quark exchange—the functions $D_\pm$ possess a nonzero imaginary part due to the Landau damping mechanism. In the real-time framework it is obtained with the help of Feynman's prescription [1], here in the logarithmic function by $q^0 \to q^0 + i\epsilon q^0$:

$$\ln\frac{q^0+q}{q^0-q} = \ln\left|\frac{q^0+q}{q^0-q}\right| - i\pi\epsilon(q^0)\theta(q^2-q^{0^2}) \ . \tag{3.10}$$

In the soft region and for large values of M we simplify the kinematics as in Sec. II and approximate $p_\mu \simeq k_\mu$, $p^2 \simeq 2k\cdot q$, and do similarly for the primed variables (Fig. 3). Since the exchanged momentum is soft the Fermi distribution is expanded and approximated by $n_F(|q^0|) \simeq 1/2$. This allows one to simplify Eq. (3.2):

$$\left.\frac{dW^{\gamma\gamma}}{dM^2}\right|_{\text{soft}} \simeq \frac{e_q^4\alpha^2}{16\pi^6}N_c\int d^4q\,\theta(q^*-\tilde{q})\int\frac{d^3k}{2\omega}\int\frac{d^3k'}{2\omega'}e^{-(\omega+\omega')/T} \times \text{tr}[\not{k}i^*S(q)\not{k}'(i^*S(q))^*]\delta(k\cdot q)\delta(k'\cdot q)\delta(M^2-2k\cdot k') \ . \tag{3.11}$$

The dominant soft contribution is calculated with the effective soft quark propagator indicated by a blob in Fig. 3 and given by

$$i^*S(q) \equiv \frac{-i}{2}\left[(\gamma^0-\boldsymbol{\gamma}\cdot\hat{\mathbf{q}})\,\text{Re}\frac{1}{D_+} + (\gamma^0+\boldsymbol{\gamma}\cdot\hat{\mathbf{q}})\,\text{Re}\frac{1}{D_-}\right] . \tag{3.12}$$

This propagator makes the difference compared to the calculation in Sec. II (cf. Fig. 1), which is based on the temperature-independent free fermion propagator $i(\not{q}+i\epsilon)^{-1}$.

Equation (3.11) has the same structure as Eq. (2.7). After carrying out the trace we therefore proceed with similar steps in performing the integrations. Neglecting terms of $O(T/M)$ we derive

$$\left.\frac{dW^{\gamma\gamma}}{dM^2}\right|_{\text{soft}} \simeq \frac{e_q^4\alpha^2}{8\pi^3}N_c TM\int_0^{q^*}\tilde{q}\,d\tilde{q}\int_{-1}^{1}\frac{dx}{(1-x^2)^{1/2}}\left[\left(\frac{1-x}{1+x}\right)\left(\text{Re}\frac{1}{D_+}\right)^2 - \text{Re}\frac{1}{D_+}\,\text{Re}\frac{1}{D_-}\right]\exp\left[\frac{-M}{T(1-x^2)^{1/2}}\right] \tag{3.13}$$

by again introducing the scaled variable $x=q^0/\tilde{q}$ and by using the property

$$\mathrm{Re}\frac{1}{D_\pm(-q^0,q)}=-\mathrm{Re}\frac{1}{D_\mp(q^0,q)}\ . \tag{3.14}$$

In Eq. (3.13) the integral with respect to x has a stationary point at $x=0$ for $M/T\gg 1$: in this limit the static properties of the exchanged quark (Fig. 3) are the relevant ones. The leading term is therefore dependent on the properties [22] of the functions $D_\pm$ for small spacelike momenta, especially for $q^0=0$ and $\tilde{q}\to 0$, namely

$$\mathrm{Re}\frac{1}{D_+(0,\tilde{q})}\approx\frac{\tilde{q}(\tilde{q}^2+m_f^2)}{(\tilde{q}^2+m_f^2)^2+(\pi m_f^2/2)^2}\ . \tag{3.15}$$

Performing the integrations over x [cf. Eq. (2.12)] as well over $\tilde{q}$, the soft $\gamma\gamma$ emission rate for large invariant masses finally becomes

$$\left.\frac{dW^{\gamma\gamma}}{dM^2}\right|_{\mathrm{soft}}\simeq\frac{e_q^4\alpha^2}{4\pi^3}N_c\left[\frac{\pi MT^3}{2}\right]^{1/2}\left[\ln\frac{q^{*2}}{m_f^2}-1-\tfrac{1}{2}\ln\left[1+\frac{\pi^2}{4}\right]+\frac{1}{\pi}\arctan\frac{2}{\pi}\right]\exp(-M/T)\ , \tag{3.16}$$

keeping in mind that $M>T>q^*>m_f$.

IV. SCREENED NET THERMAL RATE

When taking into account the screening mechanism the thermal production rate for photon pairs is finally obtained by adding the hard [Eq. (2.13)] and soft [Eq. (3.16)] contributions,

$$\begin{aligned}\frac{dW^{\gamma\gamma}}{dM^2}&=\frac{dW^{\gamma\gamma}}{dM^2}|_{\mathrm{hard}}+\left.\frac{dW^{\gamma\gamma}}{dM^2}\right|_{\mathrm{soft}}\\&\simeq\frac{\sum_q e_q^4\alpha^2}{4\pi^3}N_c\left[\frac{\pi MT^3}{2}\right]^{1/2}\left[\ln\left[\frac{M^2}{m_f^2\sqrt{1+\pi^2/4}}\right]-2+\frac{1}{\pi}\arctan\frac{2}{\pi}\right]\exp(-M/T)\ .\end{aligned} \tag{4.1}$$

This is the leading-order term for large invariant masses, $M>T$, and at large temperature. The sum over quark flavors is now included in (4.1). It is explicit from this expression that the dependence on the intermediate momentum cutoff q^* disappears and an infrared stable result for the $\gamma\gamma$ emission rate follows. It may be summarized in compact form by

$$\begin{aligned}\frac{dW^{\gamma\gamma}}{dM^2}\simeq&\frac{\sum_q e_q^4\alpha^2}{4\pi^3}N_c\left[\frac{\pi MT^3}{2}\right]^{1/2}\\&\times\exp(-M/T)\ln\left[\frac{cM^2}{\alpha_s T^2}\right]\ ,\end{aligned} \tag{4.2}$$

with the constant c under the logarithm given by

$$\begin{aligned}c&=\frac{3}{\pi(4+\pi^2)^{1/2}}\exp\left[-2+\frac{1}{\pi}\arctan\frac{2}{\pi}\right]\\&\simeq 0.042\ ,\end{aligned} \tag{4.3}$$

when using the explicit form for the thermal fermion mass m_f of (3.9). We note the small numerical value of this constant.

Now we compare this result with previous calculations [8–12] based on kinetic theory, in particular with the expression given by Eq. (2.5), which does not include screening effects at all: the temperature dependence originates only from the thermal distribution functions for the quarks in the initial state of the process $q\bar{q}\to\gamma\gamma$, since the (total) cross section is evaluated at zero temperature. The mass parameter in (2.5) is interpreted as the current quark mass. In the kinematical region of invariant masses of the photon pair $M>1$ GeV and for temperatures $0.15<T<0.4$ GeV the $\gamma\gamma$ rates calculated from Eq. (2.5) are (depending on M) 3–6 times larger than the screened ones from (4.2), when a quark mass of $m=5$ MeV is used. This is illustrated in Fig. 4.

Instead of absolute predictions we present ratios to thermal lepton-pair, i.e., dimuon rates, also produced via quark-antiquark annihilation (the light u- and d-quark contributions are considered). In the limit where $M/T>1$ the $\mu^+\mu^-$ rates are well approximated by the leading-order expression [23,24], since the gluon-induced corrections are vanishingly small [25],

$$\begin{aligned}\frac{dW^{\mu^+\mu^-}}{dM^2}\simeq&\frac{2}{3}\frac{\sum_q e_q^2\alpha^2}{4\pi^3}N_c\left[\frac{\pi MT^3}{2}\right]^{1/2}\\&\times\exp(-M/T)\ .\end{aligned} \tag{4.4}$$

When considering these ratios the dependence on the space-time volume drops out. Neglecting screening, the ratio becomes temperature independent, and it is shown by the long-dashed curve in Fig. 4. With screening, a

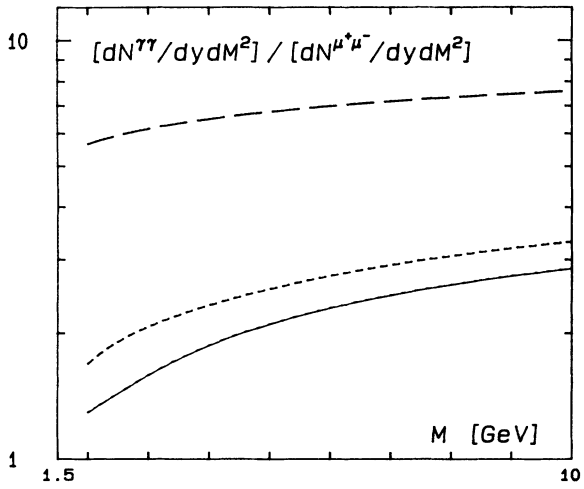

FIG. 4. The thermal $\gamma\gamma$ rates normalized to $\mu^+\mu^-$ spectra [Eq. (4.4)] as a function of the invariant mass of the produced pairs. The long-dashed line is calculated from Eq. (2.5) where the screening mechanism is neglected in the calculation of the $\gamma\gamma$ emission rate. The two lower curves are calculated with the correct treatment of screening [Eq. (4.2)] as explained in the text. The dashed line corresponds to $T=200$ MeV (for O+Au collisions at CERN SPS energy), the solid line to $T=300$ MeV (for Pb+Pb collisions at LHC energy).

weak logarithmic temperature dependence [cf. (4.2)] remains, which is plotted for $T=200$ MeV (dashed curve) and for $T=300$ MeV (solid curve) in the same figure; the strong coupling constant is fixed by $\alpha_s=0.3$. These temperatures are typical for heavy-ion collisions under present discussion.

We remark that the constant c in Eq. (4.3) is smaller by a factor of ~ 4 than the constant $3/2\pi e$, which one may obtain by roughly estimating the screening effect on the $\gamma\gamma$ emission rate by replacing the mass parameter m in Eq. (2.5) by the thermal mass m_f. However, in this case the Landau damping effect is not properly taken into account. In summary the previous estimates significantly overestimate the $\gamma\gamma$ emission rate in comparison to Eq. (4.2).

V. TRANSVERSE MOMENTUM AND ANGULAR DISTRIBUTIONS OF PHOTON PAIRS

In this section we briefly summarize a few results on differential rates for photon pairs, which are defined in close analogy to the ones familiar from thermal lepton pairs produced in a hot quark-gluon plasma [3].

We first consider the transverse (with respect to a fixed direction in the isotropic plasma) momentum distribution of $\gamma\gamma$ pairs [12]. Taking the sum of the photon momenta, $\mathbf{k}+\mathbf{k}'$, and keeping its transverse projection fixed (denoted by p_T), we investigate the differential rate for large-mass pairs $M \gg T$, and with $p_T \ll M$: in this limit the integrations may be performed analytically following similar steps already described in Secs. II and III. Again screening of the quark mass singularity is dominated by the static properties of the quark propagator [cf. Eq. (3.15)]. The final expression for the rate with respect to p_T factorizes into

$$\frac{dW^{\gamma\gamma}}{dM^2 dp_T^2} \simeq \frac{e^{-p_T^2/2MT}}{2MT} \frac{dW^{\gamma\gamma}}{dM^2} . \tag{5.1}$$

The p_T dependence, i.e., the shape, is simply determined by a Gaussian factor, and therefore is not affected by screening effects, which are all contained in the integrated rate $dW^{\gamma\gamma}/dM^2$ as given by Eq. (4.1).

Hirasawa, Kadoya, and Miyazaki [11] propose to measure the angular distribution of the photon pairs at fixed invariant masses M. Since the conclusions of Ref. [11] are based on calculations that do not include screening of the quark mass singularity, we estimate the production rate in the limit $M \gg T$. Expressing the angle θ between the photon momenta in terms of M and the photon energies (cf. Sec. II) by

$$\cos\theta = 1 - \frac{M^2}{2\omega\omega'} , \tag{5.2}$$

we find for the leading term—as for Eq. (5.1)—a factorized expression

$$\frac{dW^{\gamma\gamma}}{dM^2 d\cos\theta} \simeq \frac{M \exp\left[-\frac{M}{T}\left[\frac{1}{\sin\theta/2}-1\right]\right]}{4T} \frac{dW^{\gamma\gamma}}{dM^2} . \tag{5.3}$$

It is valid for large θ, $\theta > \pi/2$, for predominantly back-to-back pairs, which is the favored configuration at large M.

Similar to the result discussed in Sec. IV we conclude from Eq. (5.3) that there is a significant reduction of the prediction after including screening. Therefore we do not share the optimistic point of view stated in Ref. [11] about the angular $\gamma\gamma$ distribution being a tool to disentangle the quark-gluon plasma from the hadron gas formed in heavy-ion collisions. The rate (5.3) is comparable in shape and magnitude to the one for $\gamma\gamma$ pairs produced in the pion phase as calculated in Ref. [11].

VI. PHOTON PAIR PRODUCTION IN AN EXPANDING QUARK-GLUON PLASMA

We have calculated thermal rates for photon pairs produced in a quark-gluon plasma at rest. We have noted that the screening effects due to the medium change these rates—in magnitude and with respect to the temperature dependence—in comparison with the ones discussed before [8–12]. Therefore a reanalysis of the predictions for $\gamma\gamma$ pairs produced in an expanding matter system seems to be necessary when having in mind possible phenomenological applications to heavy-ion collisions.

In this case the production rates $W^{\gamma\gamma} \equiv dN^{\gamma\gamma}/d^4x$ have to be integrated over the complete space-time history of the quark-gluon plasma. In order to obtain representative predictions we apply the model by Bjorken [26] for longitudinal hydrodynamical expansion and we assume a first-order deconfinement phase transition. Modifications due to transverse expansion are expected to

be small [27]. The space-time volume element is expressed as

$$d^4x = d^2x_T dy \tau d\tau \ , \tag{6.1}$$

where τ is the proper time, y the rapidity of the plasma element, and x_T its transverse coordinate.

For central heavy-ion $A+A$ collisions the integration over x_T gives a constant factor πR_A^2, where $R_A \simeq 1.15 A^{1/3}$ is the nuclear radius. With the cross sections given in Secs. IV [Eq. (4.2)] and V [Eq. (5.1)], respectively, the invariant mass (and p_T) spectra of thermal $\gamma\gamma$ pairs produced in head-on $A+A$ collisions are calculated as follows [28]:

$$\frac{dN^{\gamma\gamma}}{dy\, dM^2 (dp_T^2)} = \pi R_A^2 \int_{\tau_1}^{\tau_2} \tau d\tau \frac{dW^{\gamma\gamma}}{dM^2 (dp_T^2)}(T(\tau)) \ ; \tag{6.2}$$

in the considered approximation the pair has the same (central) rapidity y as the plasma where it is produced. The dependence of temperature on τ required in (6.2) is fixed by conservation of the entropy current, which together with the ideal-gas equation of state for the quark-gluon matter implies $\tau T^3(\tau) = \text{const}$.

In order to perform the τ integration the following scenarios for the expanding quark-gluon-matter system are considered. At an initial time τ_i the system is in a pure quark-gluon-plasma phase with high initial temperature T_i. Then it cools by hydrodynamic expansion down to the critical temperature T_c. The rates of $\gamma\gamma$ pairs produced during this phase are calculated numerically from Eq. (6.2) by substituting $\tau_1 = \tau_i$ and $\tau_2 = \tau_i (T_i/T_c)^3$. Then the system remains in a mixed phase at temperature T_c until the quark-gluon plasma is totally converted into the hadron (pion) gas, which continues to expand until the temperature drops to its final value. During the mixed phase the temperature stays constant, $T = T_c$, in the same interval from $\tau_1 = \tau_i (T_i/T_c)^3$ to $\tau_2 = R\tau_1$, where $R \simeq 12$ is the ratio of the number of degrees of freedom in the quark-gluon plasma and in the pion gas. The time integration in Eq. (6.2) is easily performed in this case,

$$\left.\frac{dN^{\gamma\gamma}}{dy\, dM^2 (dp_T^2)}\right|_{\text{mixed}} = \pi R_A^2 \frac{R-1}{2} \left[\left[\frac{T_i}{T_c} \right]^3 \tau_i \right]^2 \frac{dW^{\gamma\gamma}}{dM^2 (dp_T^2)} . \tag{6.3}$$

The total $\gamma\gamma$ production rates due to the presence of a quark-gluon plasma are then given by a sum of the pure- and of the mixed-phase contributions. Here we do not discuss the hadronic-gas contributions to the rates from the mixed as well as from the pure hadronic phases.

The final results for the $\gamma\gamma$ spectra evidently depend on a number of parameters: the initial time, and the initial and critical temperatures. We take $\tau_i = 1$ fm for the value of the initial thermalization time. For isentropic longitudinal expansion the initial temperature can be estimated from its relation to the hadron multiplicity in a central $A+A$ collision [29],

$$\frac{dN}{dy} \simeq 2.5 A^{2/3} \left[\frac{T_i}{100 \text{ MeV}} \right]^3 . \tag{6.4}$$

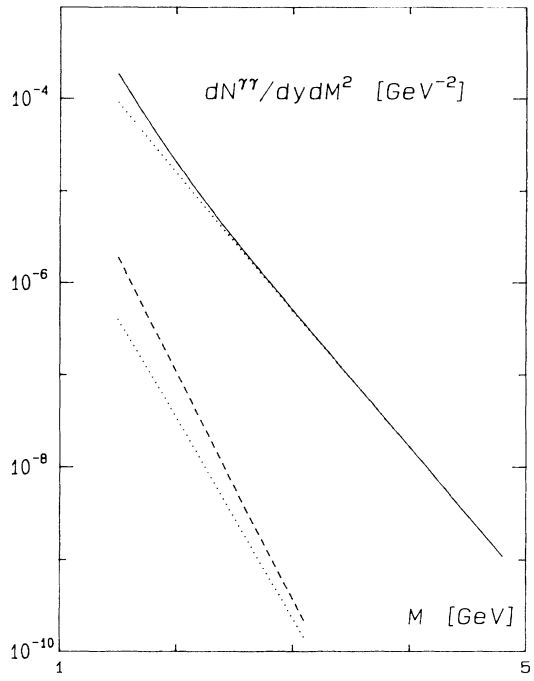

FIG. 5. Invariant-mass distribution for thermal $\gamma\gamma$ pairs for central heavy-ion collisions as discussed in Sec. VI. Dashed line corresponds to O+Au collisions at CERN SPS energy calculated with $dN/dy = 120$ and $T_i = 0.2$ GeV. Solid line describes Pb+Pb collisions at LHC energy with $dN/dy = 2200$ and $T_i = 0.3$ GeV. Dotted lines indicate the contribution from the pure quark-gluon-plasma phase.

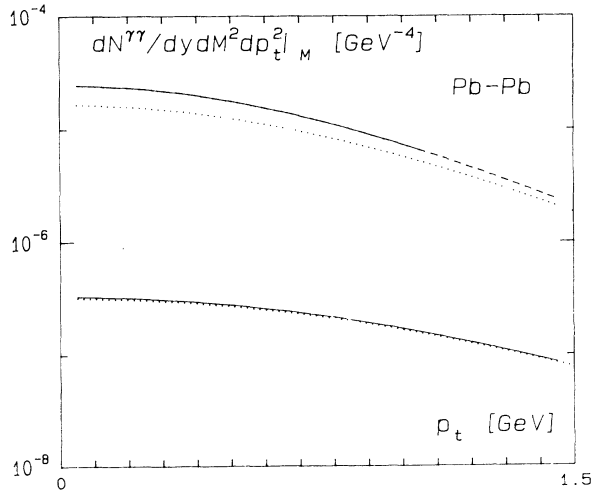

FIG. 6. Transverse momentum distribution of thermal $\gamma\gamma$ pairs for Pb+Pb collisions at LHC energy at a fixed value of the invariant mass. The lower curves are calculated with $M = 3$ GeV, the upper ones with $M = 1$ GeV. Dotted lines indicate the contribution from the pure quark-gluon-plasma phase.

Concerning T_c the most recent lattice gauge theory results [30] indicate a deconfinement temperature $T_c \simeq 150$ MeV for two quark flavors.

In the following we present the $\gamma\gamma$ spectra for central collisions between O+Au and Pb+Pb nuclei at CERN Super Proton Synchrotron (SPS) and Large Hadron Collider (LHC) energies, respectively. For these collisions one predicts hadron multiplicities to be in the range of $dN/dy \simeq 120$ for SPS and $dN/dy \simeq 2200$ for LHC energies [3], which according to Eq. (6.4) gives $T_i \simeq 200$ MeV and $T_i \simeq 300$ MeV, i.e., larger than T_c.

In Fig. 5 we show the $\gamma\gamma$ invariant-mass distributions for O + Au and Pb + Pb collisions at SPS and LHC energies. For each collision we separate from the total spectra the contribution due to the pure quark-gluon phase. A significant increase in magnitude of the spectra is observed in Fig. 5 when going from O+Au to Pb+Pb collisions, which is related to the increase of particle multiplicity dN/dy and via (6.4) to the increase of the initial temperature T_i. Explicitly this increase is due to two different effects: (i) a quadratic dependence of the production spectra on dN/dy, and (ii) with an increase in T_i the system spends more time in the pure quark-gluon-plasma phase. In this phase the exponential dependence $\exp(-M/T)$ predicts that pairs with large invariant masses are more abundantly produced at larger values of T_i: this is shown in Fig. 5 by comparing $\gamma\gamma$ pairs with $M > 2$ GeV in Pb+Pb collisions with those in O+Au collisions. For the latter the mixed-phase contribution (6.3) is still significant for pairs with masses up to $M = 4$ GeV.

In Fig. 6 we plot the transverse momentum distribution with $p_T/M < 1$ of thermal photon pairs (with masses of $M = 2$ and 3 GeV) produced in Pb+Pb collisions at LHC energy. The $\gamma\gamma$ pairs with $M = 3$ GeV are predominantly produced from the pure quark-gluon phase. This is not the case for the pairs with $M = 2$ GeV: the contribution of the mixed phase cannot be neglected, in particular when the transverse momentum p_T is small.

We close this phenomenological section with the following remark: the theoretical curves in Figs. 4–6 are calculated for a fixed value of $\alpha_s = 0.3$, which is a generally accepted value for temperatures of $T \simeq 150$–300 MeV. However, this corresponds to a rather large value of the strong-coupling constant $g_s \simeq 2$. Therefore it remains an open problem to justify the extrapolation of results to this range in the coupling, which are strictly speaking derived from the assumption that the hard-momentum-scale regime is well separated from the one with the soft scale, i.e., for $g_s T \ll T$. Only beyond-leading-order calculations may hopefully allow for a positive answer.

VII. SUMMARY

We have investigated the thermal rate of photon pairs produced in a quark-gluon plasma at high temperature. For pairs with large invariant masses we could explicitly show in leading orders of the electromagnetic as well as the strong-coupling constant how the quark mass singularity, which is present at the tree level, becomes shielded. This is achieved by including the thermal effects of the medium on the quark propagation by resumming hard thermal-loop contributions. Although originally the notion of hard thermal loops as well as the resummation procedure are based on the imaginary-time formalism, the presented results are derived in the real-time framework.

In Sec. IV we have described how our calculation gives results for the $\gamma\gamma$ rate significantly different—in magnitude and in dependence on temperature—from the ones previously obtained. This observation is already familiar from the calculations of the thermal production rate of single hard photons.

Subsequently we have studied the invariant-mass and transverse momentum spectra of the $\gamma\gamma$ pairs produced by an expanding quark-gluon plasma that is initially formed in heavy-ion collisions. The predictions are worked out in Bjorken's model. Although this description of the expansion dynamics adds new uncertainties we believe that the underlying infrared-stable rates of Secs. IV and V indeed systematically improve these predictions for the photon-pair spectra.

We do not cover in this paper the theoretically more involved but nevertheless interesting case of pairs with small invariant masses M—of the order of or less than the temperature T. Also not considered are photon pairs produced in the hadron-gas phase. However, a careful (re)analysis of these spectra seems to be required before definite conclusions may be drawn about discriminating between hadron-gas and quark-gluon-plasma phases by measuring photon pairs in heavy-ion collisions.

ACKNOWLEDGMENTS

Discussions with H. Satz are kindly acknowledged. This work was supported in part by the Ministry for Research and Technology (BMFT) of the Federal Republic of Germany under Contract No. 06-BI-701.

[1] For a review, see N. P. Landsman and Ch. G. van Weert, Phys. Rep. **145**, 141 (1987); J. I. Kapusta, *Finite-Temperature Field Theory* (Cambridge University Press, Cambridge, England, 1989); M. Le Bellac, in Proceedings of the XXXth International Universitaetswochen füer Kernphysik, Schladming, 1991 (unpublished).

[2] R. D. Pisarski, Nucl. Phys. **B309**, 476 (1988); Phys. Rev. Lett. **63**, 1129 (1989); E. Braaten and R. D. Pisarski, *ibid.* **64**, 1338 (1990); Nucl. Phys. **B337**, 569 (1990); **B339**, 310 (1990); J. Frenkel and J. C. Taylor, *ibid.* **B334**, 199 (1990); E. Braaten, in *Proceedings of QCD '90,* Montpellier, 1990, edited by S. Narison [Nucl. Phys. B (Proc. Suppl.) **23B**, 351 (1991)]; R. D. Pisarski, Nucl. Phys. **A525**, 175c (1991).

[3] For recent summary, see H. Satz, in *Proceedings of the ECFA Workshop on Large Hadron Colliders,* Aachen, Germany, 1990, edited by G. Jarlskog and D. Rein (CERN Report No. 90-10, Genève, 1990), Vol. I, p. 188.

[4] This was partially shown by K. Kajantie and P. V. Ruuskanen, Phys. Lett. **121B**, 352 (1983).

[5] J. I. Kapusta, P. Lichard, and D. Seibert, Phys. Rev. D **44**,

2774 (1991).
[6] R. Baier, H. Nakkagawa, A. Niégawa, and K. Redlich, Z. Phys. C **53**, 433 (1992).
[7] For a recent experiment, see WA80 Collaboration, R. Albrecht *et al.*, Z. Phys. C **51**, 1 (1991).
[8] R. Yoshida, T. Miyazaki, and M. Kadoya, Phys. Rev. D **35**, 388 (1987).
[9] K. Redlich, Phys. Rev. D **36**, 3378 (1987).
[10] B. Datta, S. Raha, and B. Sinha, Nucl. Phys. **A490**, 733 (1988).
[11] S. Hirasawa, M. Kadoya, and T. Miyazaki, Phys. Lett. B **218**, 263 (1989).
[12] For a review, see S. Raha and B. Sinha, Int. J. Mod. Phys. A **6**, 517 (1991).
[13] G. Staadt, W. Greiner, and J. Rafelski, Phys. Rev. D **33**, 66 (1986).
[14] E. Braaten and T. C. Yuan, Phys. Rev. Lett. **66**, 2183 (1991); E. Braaten and M. H. Thoma, Phys. Rev. D **44**, 1298 (1991).
[15] H. A. Weldon, Phys. Rev. D **28**, 2007 (1983).
[16] A Niégawa, Phys. Lett. B **247**, 351 (1990); N. Ashida, H. Nakkagawa, A. Niégawa, and H. Yokota, Phys. Rev. D **45**, 2066 (1992); Ann. Phys. (N.Y.) (to be published).
[17] R. L. Kobes and G. W. Semenoff, Nucl. Phys. **B260**, 714 (1985); **B272**, 329 (1986).
[18] V. V. Lebedev and A. V. Smilga, Ann. Phys. (N.Y.) **202**, 229 (1990); Phys. Lett. B **253**, 231 (1991); Ann. Phys. (N.Y.) (to be published).
[19] The bosonic ones are discussed by T. Altherr, Ann. Phys. (N.Y.) **207**, 374 (1991).
[20] V. V. Klimov, Yad. Fiz. **33**, 1734 (1981) [Sov. J. Nucl. Phys. **33**, 934 (1981)]; O. K. Kalashnikov, Fortschr. Phys. **32**, 525 (1984).
[21] H. A. Weldon, Phys. Rev. D **26**, 2789 (1982); Physica A **158**, 169 (1989); Phys. Rev. D **40**, 2410 (1989).
[22] R. D. Pisarski, Physica A **158**, 146 (1989); Fermilab Report No. Pub-88/113-T (unpublished).
[23] L. D. McLerran and T. Toimela, Phys. Rev. D **31**, 545 (1985).
[24] For earlier references, see G. Domokos, Phys. Rev. D **28**, 123 (1983); S. A. Chin, Phys. Lett. **119B**, 51 (1982).
[25] T. Altherr and P. Aurenche, Z. Phys. C **45**, 99 (1989); Y. Gabellini, T. Grandou, and D. Poizat, Ann. Phys. (N.Y.) **202**, 436 (1990).
[26] J. D. Bjorken, Phys. Rev. D **27**, 140 (1983).
[27] H. von Gersdorff, L. McLerran, M. Kataja, and P. V. Ruuskanen, Phys. Rev. D **34**, 794 (1986); K. Kajantie, M. Kataja, L. McLerran, and P. V. Ruuskanen, *ibid.* **34**, 811 (1986).
[28] K. Kajantie, J. Kapusta, L. McLerran, and A. Mekjian, Phys. Rev. D **34**, 2746 (1986).
[29] R. Hwa and K. Kajantie, Phys. Rev. D **32**, 1109 (1985).
[30] S. Gottlieb *et al.*, Phys. Rev. D **35**, 3972 (1987); for a recent review, see B. Petersson, Nucl. Phys. **A525**, 237c (1991).